

# Soccer line mark segmentation with stochastic watershed transform

Daniel Berjón<sup>a,\*</sup>, Carlos Cuevas<sup>a</sup>, Narciso García<sup>a</sup>

<sup>a</sup>*Grupo de Tratamiento de Imágenes, Information Processing and Telecommunications Center, Universidad Politécnica de Madrid, Spain*

---

## Abstract

Augmented reality applications are beginning to change the way sports are broadcast, providing richer experiences and valuable insights to fans. The first step of augmented reality systems is camera calibration, possibly based on detecting the line markings of the field of play. Most existing proposals for line detection rely on edge detection and Hough transform, but optical distortion and extraneous edges cause inaccurate or spurious detections of line markings. We propose a novel strategy to automatically and accurately segment line markings based on a stochastic watershed transform that is robust to optical distortions, since it makes no assumptions about line straightness, and is unaffected by the presence of players or the ball in the field of play. Firstly, the playing field as a whole is segmented completely eliminating the stands and perimeter boards. Then the line markings are extracted.

The strategy has been tested on a new and public database composed by 60 annotated images from matches in five stadiums. The results obtained have proven that the proposed segmentation algorithm allows successful and precise detection of most line mark pixels.

*Keywords:* soccer, football, line mark, segmentation, line detection, watershed

---

## 1. Introduction

Association football, more commonly known as football or soccer, is the most popular team sport in the world [1]. It is played by more than 265 million players in more than 200 countries [2]. Moreover, it is the sport with the largest television audience with nearly 4 billion followers [3].

As a consequence of this great popularity and thanks to the technological advances produced in the last decade, the demand for artificial vision applications to automatically analyze soccer matches has grown enormously in recent

---

\*Corresponding author.

*Email addresses:* `dbd@gti.ssr.upm.es` (Daniel Berjón), `ccr@gti.ssr.upm.es` (Carlos Cuevas), `narciso@gti.ssr.upm.es` (Narciso García)

years [4]. On the consumer end, spectators demand applications capable of enriching the content of live broadcasts [5]. Meanwhile on the professional side, clubs and players request applications aimed at a better understanding of the game, studying team tactics, or creating training sessions to improve player performance [6]. Additionally, the Video Assistant Referee (VAR), introduced in 2018 into the Laws of the Game of the International Football Association Board (IFAB) to help referees in reviewing decisions by means of video footage [7], has given rise to a notable increase in the technology used in the stadiums [8]. Besides, during recent years there has been a surge of interest in applications focused on accurately predicting soccer games [3].

To enable analysis of team tactics and obtain individual and global statistics, many of these applications include algorithms for detecting and tracking the players and/or the ball throughout the matches. From the positions of the players and the ball, they provide different indicators capable of describing and improving the understanding of the game [9]: distance traveled by the players of each team, distance from the ball to the goal in a free kick, positions occupied by players throughout the game, outside detection, goal opportunities, etc.

To tackle these high-level tasks, it is necessary to register the images in a model of the field of play [10] and/or calibrate the cameras [11]. The strategies with these aims are typically based on the detection of key-points of the field of play, which are determined from the intersections between the line marks on the grass [12]. These line marks can be of two types: straight lines and circles (projected into ellipses in the images). Therefore, the location of the line marks is a key stage in all these high-level tasks.

To our knowledge, all the methods proposed for locating line marks, instead of segmenting them, try to approximate them to straight line models or ellipse models. Consequently, although they are successful in simple images, they fail in several cases, such as in images containing both types of marks (i.e., straight lines and circles), or in images with radial distortion.

### 1.1. Contribution

The main contributions of this work are:

- Segmentation of the field of play. We propose a new strategy to segment the field of play, which is able of providing very accurate boundaries of the grass pitch in images taken from different viewpoints and in complex situations (e.g., lawn striping resulting from bending the grass in different directions, or outdoors high contrast illumination).
- Use of watershed transformation to eliminate irrelevant edges. Many proposals for line marking detection start from a proto-edge-detection stage that yields many unwanted edges. Unlike existing methods, we use the watershed transformation because it lends itself naturally to flood out irrelevant edges such as those due to the players or the ball.
- Seed placing strategy. Our proposal builds upon the stochastic watershed algorithm [13], but our goal is different (line marking detection instead

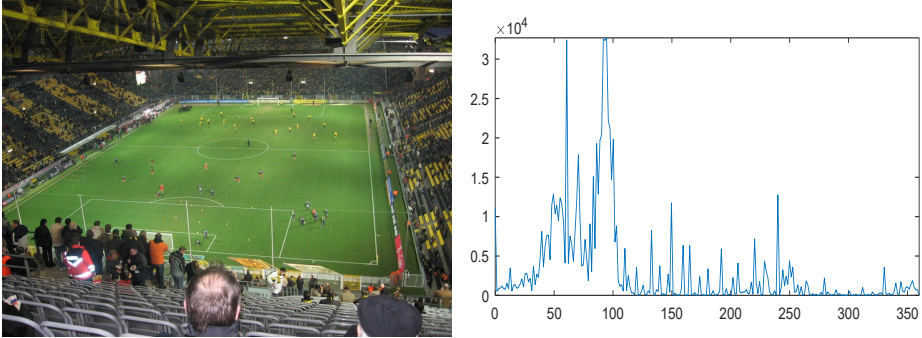


Figure 1: Example of a very complex histogram of the hue component of an image.

of region segmentation); this allows us to propose a seed placing strategy that ensures quick convergence and does not require the user to manually set the number of regions to be sought.

- Creation of a public database of annotated images of soccer matches in multiple stadiums with varied viewpoints, grass colors and illumination conditions to ease evaluation and comparison of vision-based soccer analysis algorithms.

### 1.2. Organization

The paper is organized as follows: in section 2 we review existing algorithms for field of play segmentation and line marking detection. Section 3 details the strategy proposed for segmenting the playing field. Next, in section 4, we discuss the use of the watershed transform to segment line markings and detail our proposal. Experiment results are reported in section 5 and, finally, section 6 presents the conclusions of the paper.

## 2. Related work

### 2.1. Field of play segmentation

The segmentation of the field of play is a fundamental stage in most soccer image analysis applications such as player detection and tracking, event detection, or game play analysis [4].

Some strategies analyze the histogram of the hue (H) component of the HSV color space in search of the dominant mode [14, 15, 16, 17, 18], which is assumed to correspond to the green color of the field of play. By separating this mode from the rest of the histogram data, high quality results are typically obtained. However, automatically selecting the appropriate thresholds can be very complex in some images, as hue histograms are often very multimodal (see Fig. 1). Moreover, there are cases where the dominant mode does not correspond to the color of the field of play (e.g., images showing a large amount of sky or stands in a uniform color).



Figure 2: Example of an imprecise result using the  $G > R > B$  rule.



Figure 3: Example of an imprecise result when segmenting using the green chromaticity.

In other works [19, 20, 21], the field of play, assumed to show a color distinguishable as green, is inferred as the region occupied by pixels satisfying the rule  $G > R > B$ , where  $G$ ,  $R$ , and  $B$  are the green, red, and blue components in the RGB color space. Similarly, in [22] it is established that the playing field pixels are those satisfying that  $G > R$  and  $G > B$ . The main advantage of these methods is their simplicity. However, they fail in gray or shaded areas (see Fig. 2).

Other works have also been proposed that, as an alternative to RGB or H, analyze the green chromaticity [23, 24], since it is highly invariant to illumination changes and provides an unequivocal criterion for comparing colors in terms of their closeness to green. However, the results of these works generally include areas of the billboards or stands with colors such as cyan or yellow, since the criterion they use to segment does not allow separating green from those colors (see Fig. 3).

### 2.2. Line mark detection

To measure distances and speeds of players and/or ball throughout the matches, the images need to be registered to a model of the field of play, which is typically accomplished from sets of key-points that result from intersections between line marks.

To detect straight line marks, the existing approaches apply the Hough transform to images where the line marks stand out from the rest of the elements [12]. Typically, such images are obtained by computing edges using the Sobel [20] or

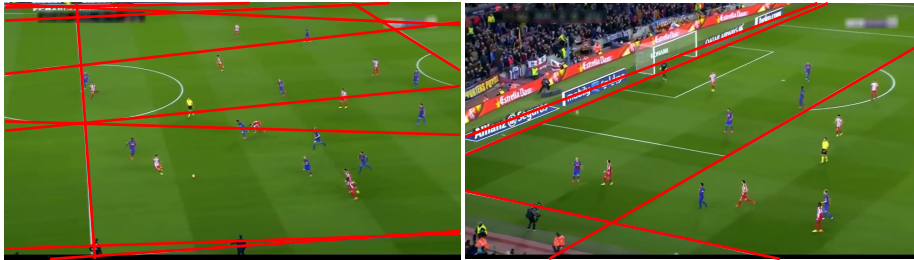


Figure 4: Examples of detected line marks superimposed on the original images.

the LoG [25] operators. These operators are computationally efficient and provide successful results in simple images. However, they are not useful in images containing edge points that do not correspond to straight line marks, but to players, ball, goals, or billboards. Moreover, some of them yield duplicate edge detections [10].

Alternatively, some authors use the Top-Hat transform to highlight the line marks in the images [26]. Thus, in contrast to strategies using the Sobel or the LoG operators, the detection of duplicate edges is avoided and, additionally, the results obtained with the Hough transform are centered in the line marks. However, in many cases they also fail due to the presence of players and billboards.

Once the Hough transform has been obtained, some strategies classify the lines according to their tilt [27]. However these analyses are limited to the cases in which the position of the camera used to acquired the images is known [28]. In other works [29, 30], the lines are classified in only two sets (longitudinal and transverse) that are used to determine the two vanishing points required for the registration. To reduce the typical misdetections when the Hough transform is applied to full images, the Hough transform is applied independently along small windows that cover the entire image in some proposals [19].

One of the main drawbacks of all these Hough-based methods is the selection of the number of lines to consider. Typically, in images captured by the Master Camera<sup>1</sup>, the maximum number of straight lines that can be seen is 10 (straight lines on each of the halves of the field of play). However, in many cases significantly fewer lines are visible. On the one hand, if the number of lines considered is too high, in images showing few straight lines several false detections will be obtained (see left image in Fig. 4). On the other hand, if the number of lines considered is too low, in images with many lines (e.g., images showing any of the goal areas), some lines will not be detected (see right image in Fig. 4).

A further drawback is that the images generally suffer from radial distortion.

---

<sup>1</sup>It is a camera placed approximately on the extension of the halfway line. It is the one used most of the time in soccer broadcasting and it is also the only considered one in most approaches in the literature.

Consequently, in some images duplicate lines are typically obtained (this can be seen on the bottom line shown in the left image in Fig. 4) and, additionally, the quality of the results of the strategies based on the detection of vanishing points is significantly decreased.

Other strategies include algorithms for registering from the detection of the center circle of the field of play [31]. Some of them use a 6-dimensional Hough transform to detect ellipses [32] since, due to the perspective of the images, the center circle is seen as an ellipse in the images. These strategies have a very high computational and memory cost [33, 34]. Additionally, since the Hough transform is also applied on edge images or Top-Hat images, their results are inaccurate because of the presence of players, billboards, etc. An additional limitation of these algorithms is that they cannot obtain successful results in images where the center circle does not appear complete. Alternatively, some authors [35] have proposed strategies using Least Squares Fitting (LSF) methods [36]. However, they are also too sensitive to the presence of data that do not belong to the ellipse.

### 3. Field of play segmentation

Before trying to detect line markings, a playing field segmentation algorithm is applied to discard irrelevant areas such as stands or digital billboards. This algorithm is an evolution of [24], which is based on the estimation of the probability density function (pdf) of the green chromaticity of the images. Although the segmentation algorithm in [24] is able of providing high-quality results in images taken from different viewpoints and in complex situations (e.g., lawn striping resulting from bending the grass in different directions, or heavily shaded stadiums), these results are not accurate enough, since they generally include part of the billboards. Moreover, these inaccuracies are especially relevant in the case of images with billboards or stands including colors such as cyan or yellow, since the criterion it uses to segment does not allow separating green from those colors. In addition, to obtain a compact final mask of the playing field, this strategy includes a region-based analysis that is highly dependent on the type of shot (i.e., on the location of the camera and the zoom used). Therefore, it depends on several thresholds.

Let  $I$  be an original RGB image of a soccer match (see Fig. 5.a). First, to integrate the white line marks in the field of play (i.e., so that the lines adopt a color similar to that of the grass that surrounds them), a morphological grayscale opening operation is applied to each primary color to obtain a new RGB image,  $I_{\text{open}}$  (Fig. 5.b). For this, a circular structuring element,  $e_{\text{sd}}$ , is used, whose diameter must be slightly greater than the width of the line marks<sup>2</sup>. In this way it is ensured that the field of play mask will be made up of a single

---

<sup>2</sup>In the images of the database we have used to assess the quality of the strategy (see Section 5) the width of the lines is between 5 and 10 pixels. Therefore, a structuring element with a diameter of 11 pixels has been used.

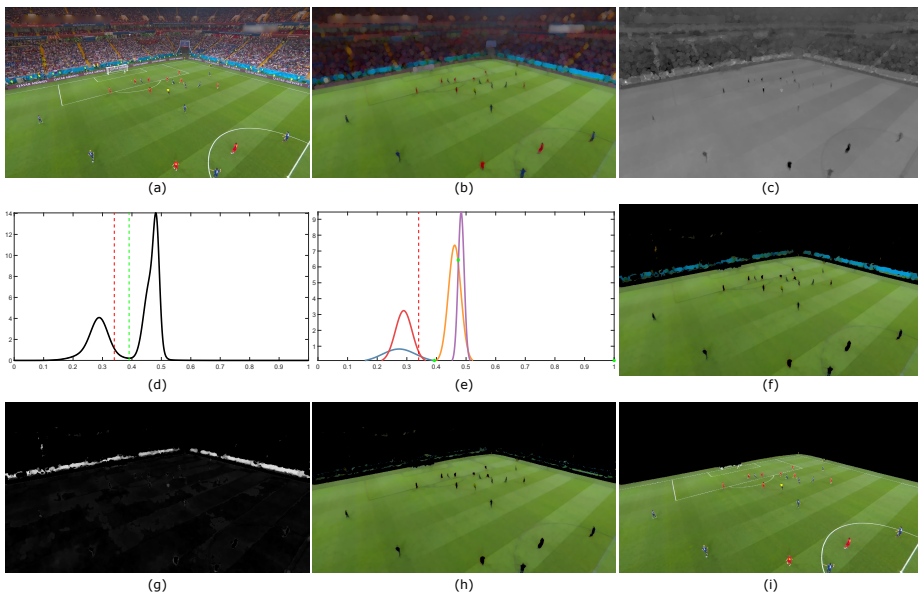


Figure 5: Main stages in the playing field segmentation strategy. (a) Original image,  $I$ . (b) Opened image,  $I_{\text{open}}$ . (c) Green chromaticity,  $g$ . (d) Estimated pdf, where the red and green dotted lines indicate, respectively, the values of  $g = 1/3$  and  $g = T_g$ . (e) Set of Gaussians used to estimate the pdf, where the green dots indicate the local minima of their envelope. (f) Initial segmentation:  $\hat{M}_{\text{PF}}$  mask applied to  $I_{\text{open}}$ . (g) Chromaticity distortion,  $cd$ . (h) Segmentation after filtering according to the  $cd$  values:  $\tilde{M}_{\text{PF}}$  mask applied to  $I_{\text{open}}$ . (i) Final segmentation,  $M_{\text{PF}}$  mask applied to  $I$ .

connected region and, therefore, deciding the number of regions to consider after segmentation is avoided.

Second, the green chromaticity of  $I_{\text{open}}$  is obtained as  $g = G/(R + G + B)$  (Fig. 5.c). Assuming that green is the dominant color of the playing field (i.e.,  $G > R + B$ ), the pixels that constitute it must meet that  $g > 1/3$ . Then, the pdf of the green chromaticity values is approximated using the Expectation-Maximization (E-M) algorithm from sets of different amounts of Gaussian distributions<sup>3</sup>, which are initialized with equal weights and with means uniformly distributed over the data range. The Akaike information criterion (AIC) [37] is finally used to select the set of Gaussians that provide the best fitting. In the example illustrated, the estimated pdf (Fig. 5.d) shows two peaks, one corresponding to the green data (i.e., pixels with  $g > 1/3$ ) and the other corresponding to the remaining colors, which are easily separable. Additionally, in Fig. 5.e it can be seen that four Gaussian distributions have been used, and that only two of them represent green data (one Gaussian for each grass shade).

An initial mask of the playing field,  $\hat{M}_{\text{PF}}$ , can be obtained selecting as threshold  $T_g$  the value of the first local minimum of the estimated pdf that is above  $1/3$  (green dotted line in Fig. 5.d). However, as it can be seen in Fig. 5.f, not only green tones but also other colors (e.g., cyan or yellow) fulfill that  $G > R + B$ , so a more sophisticated strategy is necessary. We can define the set  $V = \{\mathbf{v}_i\}_{i=1}^{N_v}$  of representative RGB colours of the grass as follows:

1. In the envelope of the Gaussian distributions that have been used for the estimation of the pdf, the set of local minima above  $T_g$  are selected,  $\{m_g\}_{i=1}^{N_v}$ . In the example illustrated in Fig. 5.e, there are two local minima, depicted as green dots at  $g = 0.39$  and  $g = 0.47$ .
2. Each element  $\mathbf{v}_i \in V$  is obtained by averaging the RGB colors of the pixels of  $I_{\text{open}}$  with values of  $g$  being between consecutive pairs of local minima and between the last local minimum and  $g = 1$ . In the example, there are  $N_v = 2$  representative RGB colors of the grass.

Then, we can rule out the unwanted colors by comparing each pixel, discounting lightness, to the elements of  $V$ . For each pixel of  $I_{\text{open}}$  we compute a chromaticity distortion value,  $cd$ , as:

$$cd = \min \{|\mathbf{u} - (\mathbf{u} \cdot \hat{\mathbf{v}}_i) \hat{\mathbf{v}}_i| \mid \mathbf{v}_i \in V\}, \quad (1)$$

where  $\mathbf{u}$  is the RGB color of said pixel. Therefore, the  $cd$  values indicate how different the chroma of each pixel is, compared to the average colors of the playing field, represented by the colors in  $V$ .

The performed experiments have shown that the values of  $cd$  can be modeled as a Normal distribution,  $\mathcal{N}(\mu_{cd}, \sigma_{cd})$ . Consequently, a new mask,  $\tilde{M}_{\text{PF}}$ , can be obtained by removing the pixels in  $M_{\text{PF}}$  not matching such Normal distribution. That is [38]:

---

<sup>3</sup>Up to 8 Gaussians, since it has been found to be enough to model complex images (e.g., with different shades of green and shadows).

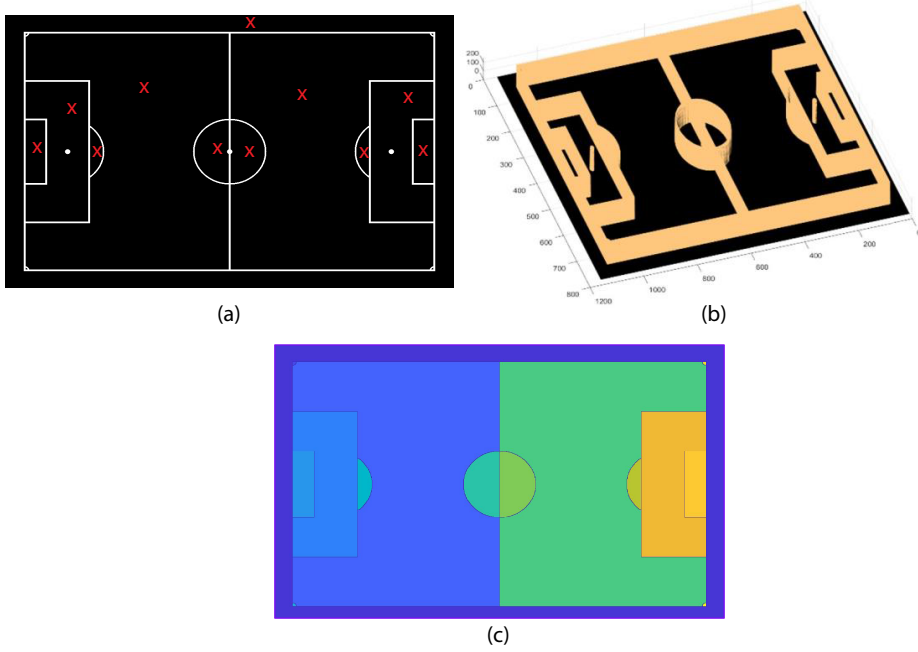


Figure 6: Example of watershed segmentation of an ideal (noiseless) image. Top left: gray-scale image with all the line markings of the field of play at a constant level; top right: segmentation results, note the disappearance of the penalty spots due to them each being surrounded by a single body of water; bottom: 3D representation of the grayscale image as an elevation map.

$$|cd - \mu_{cd}| > 3\sigma_{cd} \quad (2)$$

As it can be seen in Fig. 5.g, the values of  $cd$  corresponding to the billboards are significantly higher than the remaining ones, and consequently most of them do not appear in  $\tilde{M}_{PF}$  (Fig. 5.h).

The final mask,  $M_{PF}$ , is obtained by filling the holes in  $\tilde{M}_{PF}$  and selecting the largest region from the resulting ones (Fig. 5.i). Note that the described strategy for segmenting the playing field is completely automatic and it does not require any manually selected threshold.

## 4. Watershed segmentation

### 4.1. Classical watershed segmentation

The watershed transform is, in its basic form, an unsupervised segmentation method based on the idea that gray-scale images can be interpreted as topographic maps, where the gray level of each pixel denotes its elevation. Thus, watershed segmentation algorithms aim to find the lines that run along the tops of ridges [39], dividing the *land* into different catchment basins; all the pixels

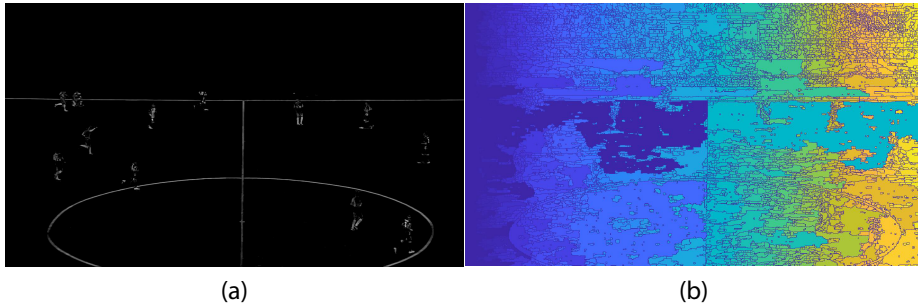


Figure 7: Example of oversegmentation resulting from unsupervised watershed segmentation. On the left, the input grayscale image; on the right, the segmentation result.

belonging to the same basin are labelled together, producing a segmentation of the input image.

There are two main algorithmic approaches to the problem, those based on flooding the image by progressively raising the water level and placing the watershed lines whenever two previously disjoint water bodies meet [40, 41, 42], and those based on terrain slope, which place a drop of water on each pixel and follow it down the slope until it reaches a minimum, so that all pixels that converge to the same minimum constitute a catchment basin [43]. When applied to ideal images such as that depicted in Fig. 6, this results in a perfect segmentation of all the closed areas independently of the intensity level of the watershed lines. Unfortunately, every local minimum, however inconspicuous, is a catchment basin. Hence, all these methods in their pure form suffer from severe oversegmentation due to capture noise, as illustrated in Fig. 7.

Recognizing this limitation, most existent watershed transform algorithms have semi-automatic variants [42], collectively known as seeded or marker-controlled watershed segmentation, which enable the user to determine the location of the relevant minima of the topographic map (think drilling wells at those locations). Then, regular watershed segmentation is performed, but whenever two catchment basins meet, instead of drawing a watershed line separating them, they are joined unless each contains a different marker. Thus, the process determines exactly as many regions as markers.

The first obvious problem with this approach is that it requires manual intervention or a supplementary algorithm to determine how many markers are necessary and where should they be located, which presumes some kind of knowledge about the image. Indeed, as Fig. 8 clearly illustrates, if no seeds are placed in a region, it will be joined, totally or in part, to adjacent ones; conversely, whenever two (or more) markers are placed together within the boundaries of what should be segmented as a single region, artificial watershed lines arise that divide the region. However, in the absence of prominent ridges, the shape of these spurious watershed lines is determined largely by noise in the image and is very sensitive to the position of the markers.

Figure 9 shows an example where the watershed lines change dramatically

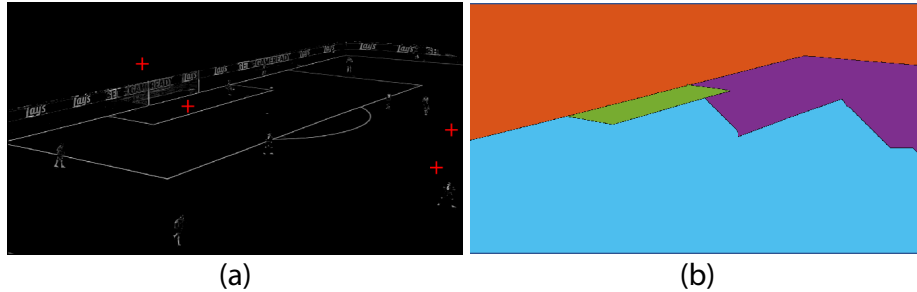


Figure 8: Left: grayscale image and four markers (yellow dots). Note that there are no markers inside the penalty box or the penalty arc, but there are two outside. Right: Segmentation result exhibiting spurious watershed lines and failing to delimit either of the unmarked regions.

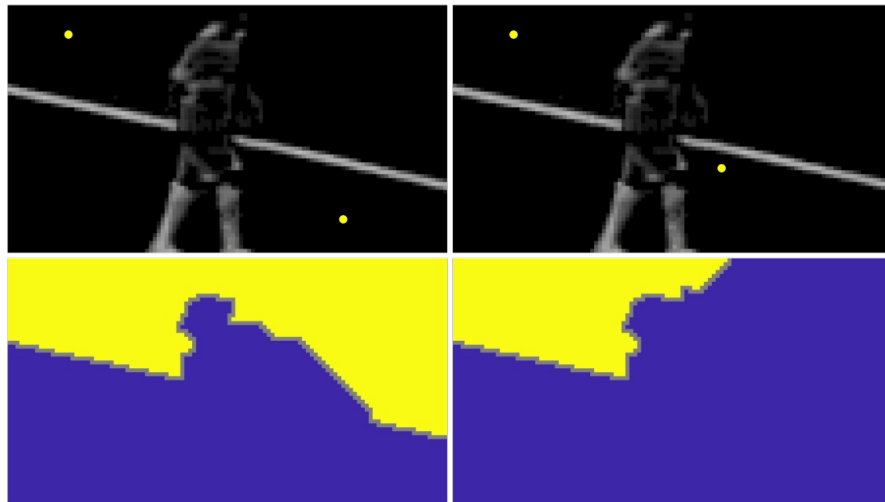


Figure 9: Examples of different segmentation results (bottom) depending on the position of the seeds (top). Note that although a human observer interprets as clearly distinct areas those above and below the line marking, they are actually joined due to the interference of the player.

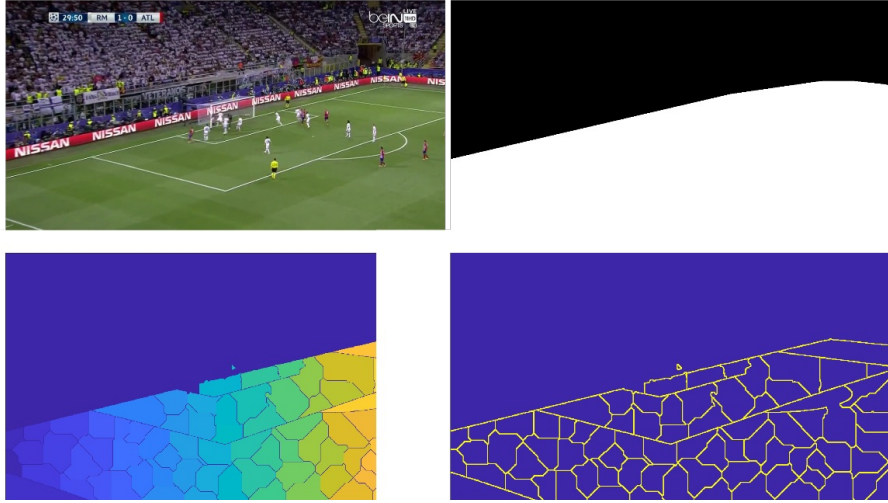


Figure 10: Left to right, top to bottom: original image,  $I$ ; field of play mask,  $M_{PF}$ ; regions determined by a single experiment of stochastic watershed segmentation; corresponding boundaries.

depending on the position of the markers. It also illustrates a less obvious problem: even when seeds are correctly placed into what we as humans identify as separate regions, if the ridges that divide these regions are interrupted or not prominent enough at some point, the water will flow across the (only implied) ridge that should separate the regions, effectively displacing the watershed line to unpredictable locations. However, the instability of spurious watershed lines can also be exploited, as proposed by the stochastic watershed method [13, 44]. The basic idea is that if a number of markers, ideally greater than the number of regions, are placed at random on the image to be segmented, the results will be a combination of true and spurious watershed lines; by repeating the experiment a number of times, true lines will appear far more often than each of the individual spurious lines, thus enabling to determine a probability density function of the watershed lines by averaging the results of the experiments. However, this algorithm still requires the user to determine the number of relevant regions, careful tuning of the distribution used to generate random seeds [45], and does not cope well with leaky region boundaries such as the one depicted in Fig. 9.

#### 4.2. Proposed watershed-based line segmentation

We propose a completely automatic procedure based on stochastic watershed to detect the line markings in a soccer pitch, provided that the playing area has already been determined, as explained in Section 3. Note that, in contrast with most watershed techniques, we are not interested in the regions themselves but in the lines that delimit them, even if they are broken as the one shown in Fig. 9. The basic idea is that, since the line markings are brighter than their surroundings, if we manage to place *numerous* markers distributed throughout

both sides of every line mark, the result will be an oversegmented image whose watershed lines will include (almost) every portion of the line markings we want to detect, and these will furthermore be the only stable watershed lines upon repetition of the experiment with different sets of markers, most of the rest being spurious lines due to an excessive number of markers. Fig. 10 shows an example of a single experiment whose results clearly exhibit most of the line markings we are looking for, where even lines interrupted by players (e.g., the penalty arc) are present at both sides of the interruption.

Let  $I_{GS}$  be the grayscale image to segment (more details will follow in section 4.2.1), with a resolution of  $H$  rows and  $W$  columns. A possible first approach is to simply generate sets of  $N$  seeds uniformly distributed across the image:

$$S_i = \left\{ \mathbf{s}_{i,j} = \begin{bmatrix} r_{i,j} \\ c_{i,j} \end{bmatrix} : \begin{array}{l} r_{i,j} = \mathcal{U}(1, H), \\ c_{i,j} = \mathcal{U}(1, W), \\ j \in \{1, 2, \dots, N\} \end{array} \right\}, \quad (3)$$

where  $r$  and  $c$  are the row and column coordinates where each seed  $\mathbf{s}$  is placed, and  $i$  identifies each individual watershed experiment; let us notate the standard seeded watershed transform on image  $I$  with the set of seeds  $S$  as  $\text{SeededWS}(I, S)$ , yielding a binary image where the pixels corresponding to watershed lines are set to 1 and all others are set to 0. Thus, we can compute

$$I_{RWS} = \frac{1}{M} \sum_{i=1}^M \text{SeededWS}(I_{GS}, S_i), \quad (4)$$

where  $M$  is the number of experiments. We can interpret the value of each pixel of  $I_{RWS}$  as akin to the probability of it being a true watershed line of  $I_{GS}$ . Since we are interested in robust line detection, the final boundary mask  $M_B$  will only consider as positive detection pixels with values exceeding a threshold  $T_{RWS}$  (henceforth  $T_{RWS} = 0.8$ ) and located within our region of interest:

$$M_B(r, c) = \begin{cases} 1, & I_{RWS}(r, c) \geq T_{RWS} \wedge M_{PF}(r, c) = 1; \\ 0, & I_{RWS}(r, c) < T_{RWS} \vee M_{PF}(r, c) = 0. \end{cases} \quad (5)$$

However, distributing seeds uniformly across both rows and columns does not guarantee that every region of the image is covered, as Fig. 11 shows: using a relatively small number of seeds has a non-negligible chance of leaving regions uncovered, leading to misdetected lines. Line misdetection can be solved either increasing the number of seeds or the number of experiments, but the former increases false detections and, while the latter does produce correct results, it does so at significantly higher cost.

To deal with these problems, we propose a windowed random seed generation which will ensure that all the regions of the image contain seeds, attaining quick convergence without increasing the rate of false detections. Let us divide the input image  $I_{GS}$  into a lattice of  $N_r$  vertical divisions and  $N_c$  horizontal divisions that will delimit  $N_r \times N_c$  non-overlapping rectangular regions (w.l.o.g., let us

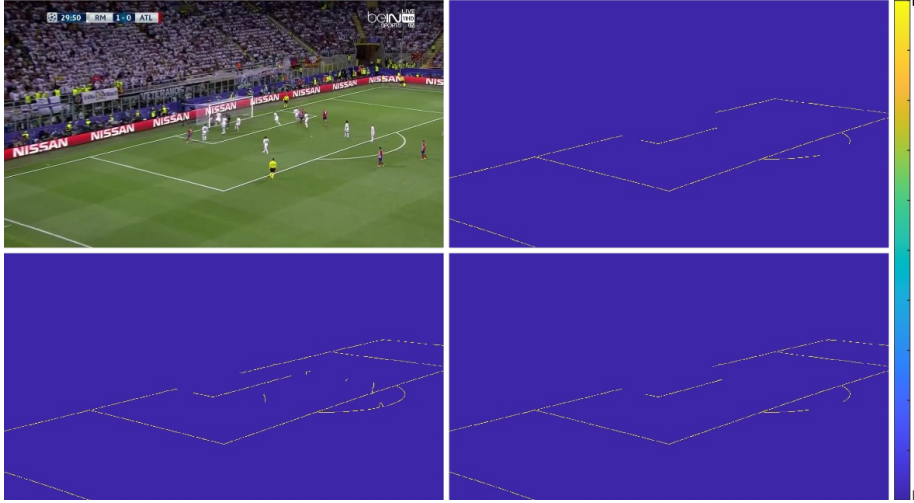


Figure 11: Results applying stochastic watershed with uniform seed distribution for different numbers of seeds and experiments. Top left: original input; top right: few experiments and few seeds ( $M = 20, N = 200$ ); bottom left: few experiments and many seeds ( $M = 20, N = 1000$ ); bottom right: many experiments and few seeds ( $M = 100, N = 200$ ).

assume  $H$  and  $W$  are divisible by  $N_r$  and  $N_c$  respectively to simplify notation); then we will place a single seed with uniform distribution into each of these regions. Thus, we replace equation 3 with

$$S_i = \left\{ \mathbf{s}_{i,j,k} = \begin{bmatrix} r_{i,j,k} \\ c_{i,j,k} \end{bmatrix} : \begin{array}{l} r_{i,j,k} = 1 + \text{mod}\left(r_{o,i} + \frac{jH}{N_r} + \mathcal{U}\left(1, \frac{H}{N_r}\right), H\right), \\ c_{i,j,k} = 1 + \text{mod}\left(c_{o,i} + \frac{kW}{N_c} + \mathcal{U}\left(1, \frac{W}{N_c}\right), W\right), \\ r_{o,i} = \mathcal{U}\left(1, \frac{H}{N_r}\right), \quad c_{o,i} = \mathcal{U}\left(1, \frac{W}{N_c}\right), \\ j \in \{0, 1, \dots, N_r - 1\}, \quad k \in \{0, 1, \dots, N_c - 1\}, \end{array} \right\}, \quad (6)$$

the rest of the procedure unchanged. Fig. 12 shows the results of this seeding method, where we can see that a small number of experiments ( $M = 20$ ) already yields results comparable to those obtained with the uniform seed generator for  $M = 100$ . Furthermore, we can also see that increasing significantly the number of experiments does not yield significant advantages. If the lattice used to generate seeds has the same origin in every experiment (e.g.,  $r_{o,i} = c_{o,i} = 0$ ), the procedure yields results which exhibit a faint yet definite pattern, roughly shaped like the lattice, in flat areas of  $I_{GS}$ , as illustrated in Fig. 12; although this effect does not actually affect results, it is easy to eliminate by using a different origin for the lattice in each experiment, as proposed.

The proposed seed location algorithm guarantees a bounded distance between seeds, like the iterative Poisson disk sampling [46], but it has a substantially lower cost and is more amenable to parallelization.

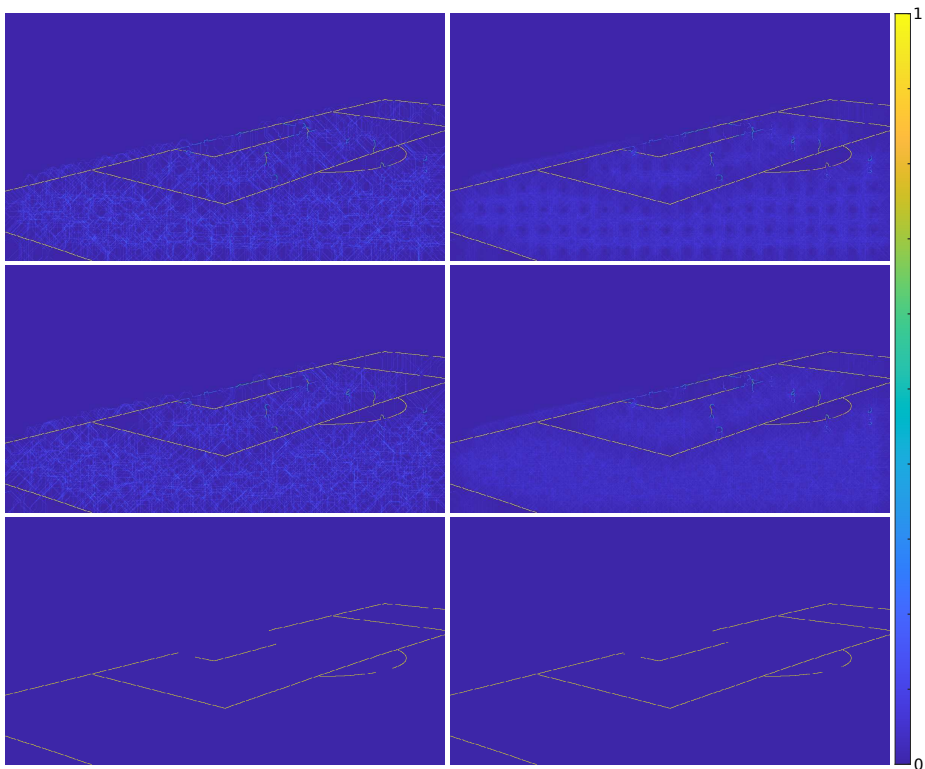


Figure 12: Results applying stochastic watershed with windowed random seed generation. On the left,  $M = 20$ ; on the right,  $M = 200$ . Rows: fixed lattice across experiments (top), proposed approach with different origin in each experiment (middle) and proposed approach after thresholding (bottom).



Figure 13: Example of false contours due to abrupt illumination changes when performing a local thresholding operation.

#### 4.2.1. Preprocess of the input image

As stated in the beginning of the previous section, it should reasonably be possible to use as input  $I_{GS}$  the brightness of the RGB input image  $I$  because the line markings have a higher brightness than their surroundings. However, in practice this results in many false detections because the marker-based watershed transform *will* find watershed lines between markers, and some configurations of texture or capture noise, even if faint, can form ridges that yield persistent watershed lines across experiments. A simple solution is to apply a local thresholding operator [47] to remove the noisy areas before applying the watershed stage.

However, in the face of abrupt illumination changes this approach is less than ideal because it may create false contours, which will then be detected as watershed lines, as illustrated in Fig. 13. The solution we have adopted is previously applying the top-hat transform [48] with the same structuring element  $e_{sd}$  defined in Section 3, which only preserves thin areas lighter than their surroundings and therefore does not exhibit this problem.

Finally, we have found that, while the brightness channel of the RGB input images is a reasonable choice because the watershed transform filters out most players anyway, it can be helpful to use  $I_{GS} = \min(R, G, B)$  since the lines, being white, are bound to have higher values than their surroundings on all three channels, while other elements like players not necessarily, decreasing the amount of possible false watershed lines.

## 5. Results

### 5.1. Labeled Soccer Database (LaSoDa).

To assess the quality of the proposed strategy, we have created a new and public database named LaSoDa<sup>4</sup>. As far as we know, there is only one other database that, like ours, allows the evaluation of the quality of algorithms to detect or segment line marks in images of soccer matches [30]. However, this

<sup>4</sup><http://www.gti.ssr.upm.es/data/>

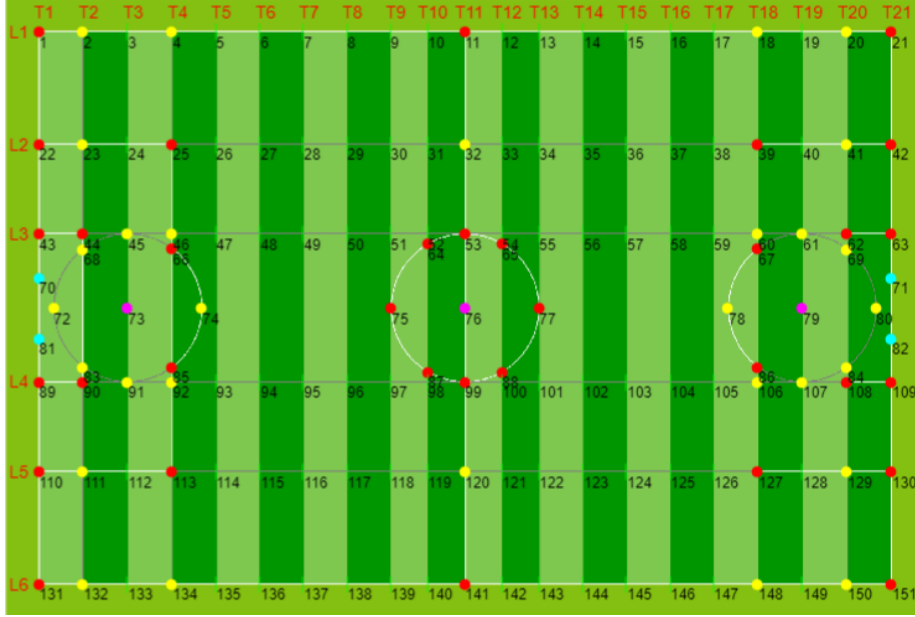


Figure 14: Field of play model used in LaSoDa.

database is not as complete as the one proposed, since all its images have been acquired with the Master Camera<sup>5</sup> and, although they belong to nine different stadiums, most of the images employ a similarly wide view angle.

LaSoDa is composed by 60 annotated images from matches in five stadiums with different characteristics (e.g., positions of the cameras, view angles, grass colors) and light conditions (day and night).

The main characteristics of this set of images are the following:

- Their content exhaustively covers all areas of the field of play: the four corners and the central part.
- They show five different zoom levels: from 1 (closest zoom) to 5 (widest zoom).
- They have been acquired with four different types of cameras: master camera (MC), side camera (SC), end camera (EC), and aerial camera (AC).
- They include different and challenging lighting conditions: day and night matches, and some heavily shaded images.

<sup>5</sup>It is the one used most of the time in soccer broadcasting. It is placed approximately on the extension of the halfway line. It performs pan, tilt, and zoom movements, but not rotations around its longitudinal axis (i.e., no roll).

### 5.1.1. Field of play model

The images in LaSoDa correspond to matches played in stadiums with the field markings established by the “Laws of the Game” of the IFAB [7]. According to these rules, the model of the field of play with which the LaSoDa images are related to is the one depicted in Fig. 14, which is characterized by 151 key points that correspond to:

- 6 longitudinal straight lines (indicated with an L).
- 21 transverse straight lines (indicated with a T).
- 3 circular lines (indicated with a C).

This model of the field of play and the coordinates of the 151 key points are included in the downloadable files of the database.

### 5.1.2. Ground truth description

For each image in the database, we provide a .MAT file (Matlab format) with its ground truth, whose content is the following:

- WLM - White Line Marks: Structure of cells where each row provides the information of one of the white lines in the image.
  - The second column contains the list of indexes indicating which pixels belong to the line.
  - The first column indicates the identifier of the line (detailed in Table 1).
- GLM - Grass Line Marks: Structure of cells where each row provides the information of one of the lines in the image that separates the grass bands resulting from bending the grass in different directions.
  - The second column contains the list of indexes indicating what pixels are part of the line.
  - The first column indicates the identifier of the line which, as can be seen in the model of the field of play, can be one of the following: T2, T3, ..., T10, T12, T13, ..., T20.
- Hom:  $3 \times 3$  matrix that corresponds to the homography transformation that allows transforming the original image to the canvas of the field of play model.
- Mask: Binary mask indicating what area of the image corresponds to the field of play.

Figure 15 shows some representative images of the database, with the ground truth superimposed.

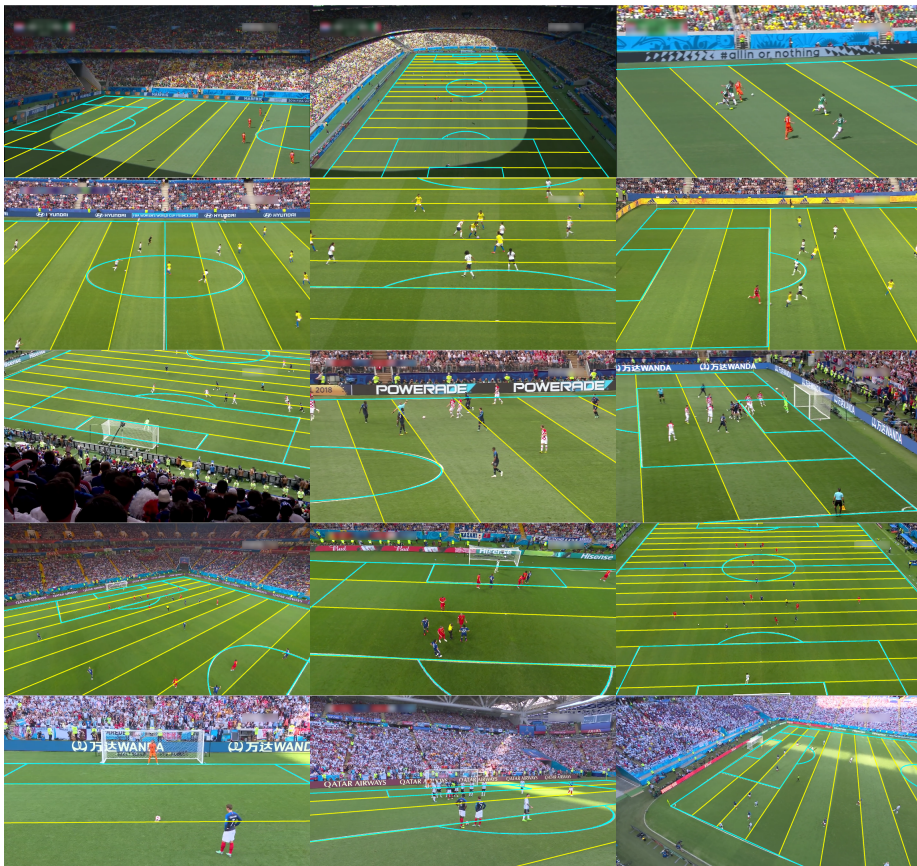


Figure 15: Representative images of the used database.

Longitudinal	
L1	Top touchline
L2_L	Top line of the left penalty area
L2_R	Top line of the right penalty area
L3_L	Top line of the left goal area
L3_R	Top line of the right goal area
L4_L	Bottom line of the left goal area
L4_R	Bottom line of the right goal area
L5_L	Bottom line of the left penalty area
L5_R	Bottom line of the right penalty area
L6	Bottom touchline
Transverse	
T1	Left goal line
T2	Left goal area line
T4	Left penalty area line
T11	Halfway line
T18	Right penalty area line
T20	Right goal area line
T21	Right goal line
Circular	
C1	Left penalty arc
C2	Centre circle
C3	Right penalty arc

Table 1: Identifiers used for the white line marks in the playing field model.

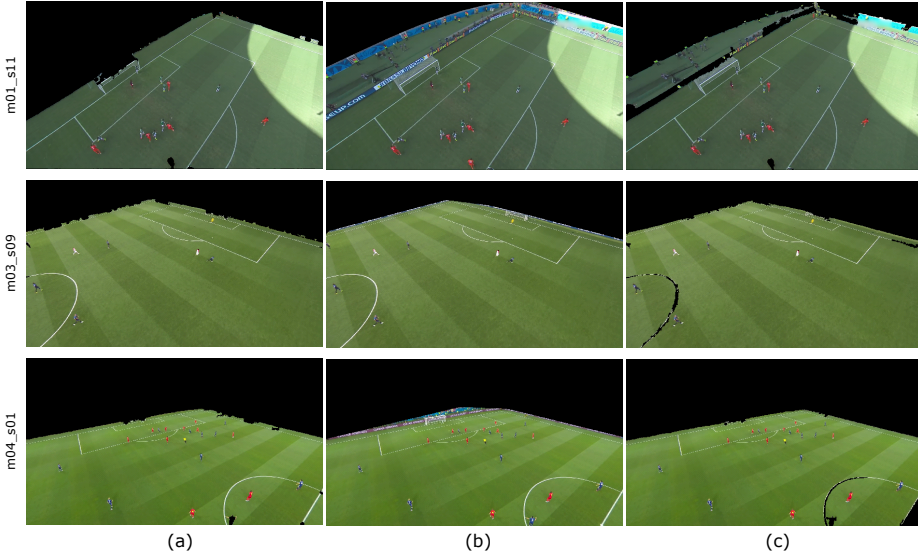


Figure 16: Representative playing field segmentation results obtained with: the proposed strategy (a), the strategy in [24] (b), and the the strategy in [17] (c).

### 5.2. Field of play segmentation

First we have assessed the performance of the playing field segmentation block alone. To that end, its results have been compared with those obtained by the segmentation strategies described in [24] and [17]. Some representative results are illustrated in Fig. 16.

The strategy described in [24], which has been taken as a starting point to develop the one proposed in this paper, fails in images with billboards with colors that cannot be correctly filtered in the green chromaticity color space (e.g., yellow or cyan). Additionally, it includes a region-based postprocessing analysis that depends on several thresholds (mainly to determine the sizes of structuring elements that are used to apply opening and closing morphological operations). Unlike this method, the proposed algorithm avoids segmenting the billboards and, in addition, it does not require selecting thresholds.

Regarding the strategy in [17], it is based on the analysis of the hue data of the image. It first computes the hue histogram of the image and searches for a peak in it. Then, it thresholds the image around such peak. Although the analysis of the hue data allows a better separation of green from other colors, automatic selection of appropriate thresholds is much more complex for hue histograms than for green chromaticity histograms (hue histograms are more noisy and requires two thresholds instead of one) [24]. Consequently, as it can be seen in the first example of Fig. 16, the results obtained with this method are less accurate than ours. In addition, in many images, hue-based methods fail to include white line marks in the mask, resulting in errors like those shown in the last two rows of Fig. 16.

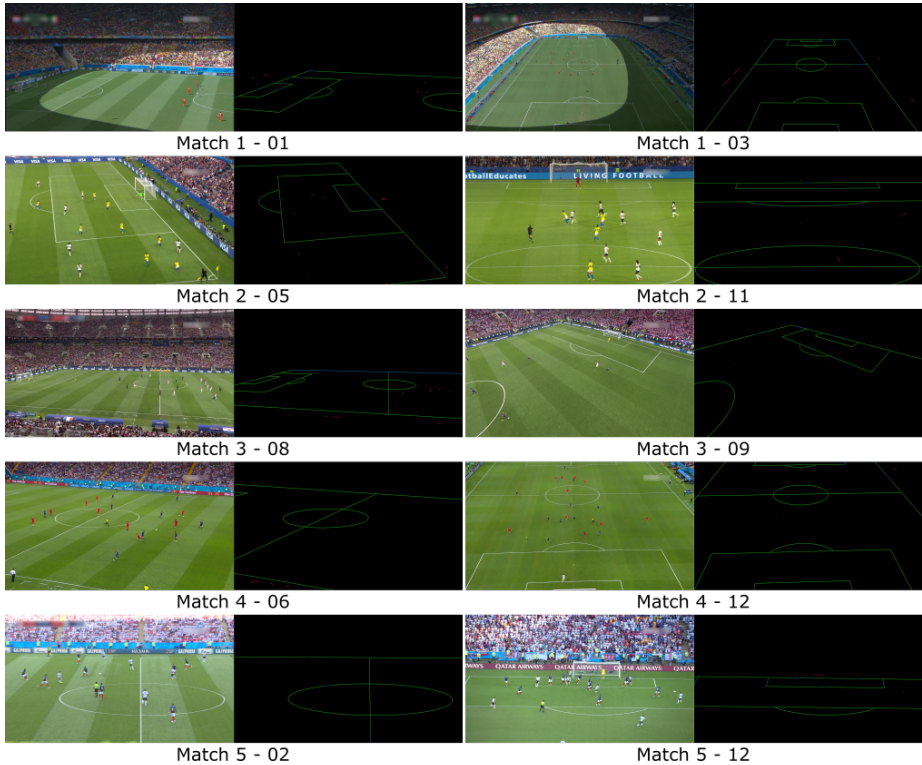


Figure 17: Some representative results obtained in the test sequences: true positives in green, false negatives in blue, and false positives in red.

### 5.3. Line mark segmentation

Next, we have evaluated the performance of the line mark segmentation method on the segmented pitch region. The quality of its results has been measured by the recall (rec), precision (pre), and F-score ( $F$ ) metrics, which are computed as:

$$\text{rec} = \frac{\text{tp}}{\text{tp} + \text{fn}}, \text{ pre} = \frac{\text{tp}}{\text{tp} + \text{fp}}, F = \frac{2\text{tp}}{2\text{tp} + \text{fp} + \text{fn}}, \quad (7)$$

where tp, fn, and fp are, respectively, the amounts of true positives, false negatives and false positives. In addition, the number of detected lines has also been taken into account compared to the total number of visible lines<sup>6</sup>. Table 2 summarizes the quality measures obtained in each of the images in the proposed database. It also shows overall quality results both for each match individually and for the entire database. Complementarily, Fig. 17 shows, for each

<sup>6</sup>A line is counted as a positive detection if at least half of its points have been detected.

of the five matches in the database, a couple of significant results (the results corresponding to the rest of the images are available on the LaSoDa website).

Table 2: Summary of results.

Match 1							
Image id.	Camera type	Zoom level	rec	pre	$F$	Detected lines	Visible lines
01	MC	4	0.91	0.97	0.94	9	10
02	MC	3	0.94	0.98	0.96	3	3
03	EC	5	0.93	0.95	0.94	19	19
04	AC	3	0.96	0.98	0.97	9	9
05	MC	3	0.99	0.95	0.97	3	3
06	MC	4	0.87	0.93	0.90	7	7
07	MC	2	0.88	0.96	0.92	8	8
08	MC	3	0.96	0.96	0.96	8	8
09	MC	4	0.95	0.98	0.97	10	10
10	SC	4	0.91	0.95	0.93	9	9
11	AC	4	0.99	0.90	0.94	8	8
12	MC	3	0.93	1.00	0.96	7	7
Match 2							
Image id.	Camera type	Zoom level	rec	pre	$F$	Detected lines	Visible lines
01	MC	4	0.96	0.96	0.96	3	3
02	MC	3	0.95	0.95	0.95	9	9
03	EC	5	0.96	0.98	0.97	7	7
04	AC	3	0.99	0.97	0.98	3	3
05	MC	3	0.99	0.95	0.97	10	10
06	MC	4	0.98	0.96	0.97	9	9
07	MC	2	0.89	0.99	0.94	3	3
08	MC	3	0.93	0.95	0.94	9	9
09	MC	4	0.81	0.94	0.87	4	5
10	SC	4	0.78	0.88	0.83	5	5
11	AC	4	0.96	0.99	0.97	8	8
12	MC	3	0.95	0.95	0.95	6	7
Match 3							
Image id.	Camera type	Zoom level	rec	pre	$F$	Detected lines	Visible lines
01	MC	4	0.89	0.94	0.91	11	11
02	MC	3	0.91	0.94	0.92	10	10
03	EC	5	0.93	0.92	0.93	7	7
04	AC	3	0.93	0.92	0.93	9	9
05	MC	3	0.82	0.95	0.88	11	12
06	MC	4	0.89	0.97	0.93	2	2

07	MC	2	0.97	0.97	0.97	9	9
08	MC	3	0.76	0.95	0.84	11	12
09	MC	4	0.96	0.99	0.97	10	10
10	SC	4	0.95	0.97	0.96	10	10
11	AC	4	0.97	0.88	0.92	7	7
12	MC	3	0.93	0.97	0.95	11	11
Match 4							
Image id.	Camera type	Zoom level	rec	pre	$F$	Detected lines	Visible lines
01	MC	4	0.94	1.00	0.97	11	11
02	MC	3	0.98	0.98	0.98	9	9
03	EC	5	0.99	0.98	0.99	8	8
04	AC	3	0.95	0.97	0.96	9	9
05	MC	3	0.98	0.94	0.96	8	8
06	MC	4	0.99	0.97	0.98	7	7
07	MC	2	0.98	1.00	0.99	3	3
08	MC	3	0.91	0.94	0.92	6	7
09	MC	4	0.90	0.99	0.94	10	10
10	SC	4	1.00	0.97	0.98	8	8
11	AC	4	0.98	0.97	0.97	9	9
12	MC	3	0.97	1.00	0.98	13	15
Match 5							
Image id.	Camera type	Zoom level	rec	pre	$F$	Detected lines	Visible lines
01	MC	4	0.98	0.94	0.96	6	6
02	MC	3	0.95	0.99	0.97	3	3
03	EC	5	0.98	0.97	0.97	7	7
04	AC	3	0.96	0.96	0.96	8	8
05	MC	3	0.97	0.91	0.94	4	4
06	MC	4	0.86	0.88	0.87	5	6
07	MC	2	0.76	0.88	0.82	6	8
08	MC	3	0.79	0.97	0.87	7	8
09	MC	4	0.91	0.93	0.92	9	9
10	SC	4	0.89	0.97	0.93	8	9
11	AC	4	0.94	0.71	0.81	12	12
12	MC	3	0.94	0.98	0.96	6	7
Overall							
			rec	pre	$F$	Detected lines	Visible lines
Match 1			0.93	0.96	0.94	100	101
Match 2			0.94	0.96	0.95	76	78
Match 3			0.91	0.94	0.92	108	110
Match 4			0.96	0.98	0.97	101	104

Match 5	0.91	0.93	0.92	81	87
Total	0.93	0.95	0.94	466	480

The results show that the quality of the detections is very high in all the images, with F-score values over 0.9 in most of them and over 0.8 in the remaining few, yielding a very high overall F-score. The results illustrated in Fig. 17 also show the high quality of the detections in all types of images. Regardless of the zoom level or perspective, most line points have been correctly segmented and the amount of false positives is very low. The few false positives are mainly due to two reasons: some players wear a white kit and, therefore, stand out on the playing field in a similar way to the lines; when the perspective of the image is very low (e.g., in Match 5-12), the white elements of the goal (the posters and the net) also show a similar appearance to that of the white lines on the pitch.

With respect to the quality of the results at line level (detected lines), it can be seen that 97% (466 of 480) of the lines have been detected. The misdetected ones are those that are very short (e.g., one of the longitudinal lines in the goal area in Match 1-01) or that, because of the perspective, are not distinguishable in the image (e.g., the upper touchline in Match 3-08).

It must be taken into account that, in contrast to the strategies described in section 2, we do not approximate the line marks to straight or ellipsoidal models, but we segment them at the pixel level without any preconception about their shape. Thus, our method does not suffer from errors caused by the radial distortion typically present in the input images, which limits the accuracy of the models used in said strategies.

## 6. Conclusions

We have presented a novel strategy to segment line markings in football pitches, irrespectively of camera position or orientation, and validated its effectiveness in a selection of images from several stadiums. This strategy is based on the stochastic watershed transform, which is usually employed to segment regions rather than lines, but we have shown that, coupled with the seeding strategy we propose, it provides a robust way to segment the line markings from the field of play without assuming that the lines are straight or conform to any particular pattern. Specifically, our method is able to correctly segment the curved lines that are typical of wide-angle takes due to optical distortion of broadcasting cameras or cope with the interference of players or the ball, which frequently cause errors in most methods based on the Hough transform.

To avoid the detection of lines outside the playing field (e.g., stands, perimeter boards), we have also proposed a new method to efficiently segment the playing field. This method is based on the analysis of the pdf of the green chromaticity of the images. It has shown to be able of obtaining very accurate boundaries of the playing field in all the test images, even in those with heavily shaded areas or those featuring perimeter boards with colors that are difficult to distinguish from the color of the grass.

To assess the quality of the proposed strategy, a new and public database (LaSoDa) has been developed. LaSoDa is composed of 60 annotated images from matches in stadiums with different characteristics (positions of the cameras, view angles, grass colors) and light conditions (natural and artificial).

Some improvements can be considered for future work, for instance parallelization of the watershed transform, since the regular arrangement of seeds may allow to independently compute different regions of the image, but the current proposal already constitutes a solid foundation for other stages in a sports video analysis pipeline to build upon.

### Acknowledgments

This work has been partially supported by the Ministerio de Economía, Industria y Competitividad (AEI/FEDER) of the Spanish Government under project TEC2016-75981 (IVME).

### References

- [1] A. E. Hassanien, Machine learning-based soccer video summarization system., in: International Conference in Multimedia, Computer Graphics and Broadcasting, 2018.
- [2] L. G. S. Félix, C. M. Barbosa, I. A. Carvalho, V. da F. Vieira, C. R. Xavier, Forecasting soccer market tendencies using link prediction, in: O. Gervasi, B. Murgante, S. Misra, C. Garau, I. Blečić, D. Taniar, B. O. Apduhan, A. M. A. C. Rocha, E. Tarantino, C. M. Torre, Y. Karaca (Eds.), Computational Science and Its Applications – ICCSA 2020, Springer International Publishing, Cham, 2020, pp. 663–675.
- [3] E. Eryarsoy, D. Delen, Predicting the outcome of a football game: a comparative analysis of single and ensemble analytics methods, in: Proceedings of the 52nd Hawaii International Conference on System Sciences, 2019, pp. 1107–1115.
- [4] C. Cuevas, D. Quilon, N. Garcia, Techniques and applications for soccer video analysis: A survey, *Multimedia Tools and Applications* 79 (39) (2020) 29685–29721.
- [5] C. Goebert, G. P. Greenhalgh, A new reality: Fan perceptions of augmented reality readiness in sport marketing, *Computers in Human Behavior* 106 (2020) 106231.
- [6] G. Andrienko, N. Andrienko, G. Anzer, P. Bauer, G. Budziak, G. Fuchs, D. Hecker, H. Weber, S. Wrobel, Constructing spaces and times for tactical analysis in football, *IEEE transactions on visualization and computer graphics* 27 (4) (2021) 2280–2297.

- [7] Laws of the game 2019/20, The International Football Association Board, IFAB, 2019.
- [8] M. Armenteros, A. J. Benitez, M. Á. Betancor, The use of video technologies in refereeing football and other sports, Routledge, 2019.
- [9] D. Memmert, K. A. P. M. Lemmink, J. Sampaio, Current approaches to tactical performance analyses in soccer using position data, *Sports Medicine* 47 (1) (2017) 1–10.
- [10] C. Cuevas, D. Quilón, N. García, Automatic soccer field of play registration, *Pattern Recognition* (2020) 107278.
- [11] J. Chen, F. Zhu, J. J. Little, A two-point method for PTZ camera calibration in sports, in: *IEEE Winter Conference on Applications of Computer Vision (WACV)*, IEEE, 2018, pp. 287–295.
- [12] Q. Yao, A. Kubota, K. Kawakita, K. Nonaka, H. Sankoh, S. Naito, Fast camera self-calibration for synthesizing free viewpoint soccer video, in: *IEEE International Conference on Acoustics, Speech and Signal Processing (ICASSP)*, IEEE, 2017, pp. 1612–1616.
- [13] J. Angulo, D. Jeulin, Stochastic watershed segmentation, in: *Proceedings of the International Symposium on Mathematical Morphology*, 2007, pp. 265–276.
- [14] H. Kataoka, K. Hashimoto, Y. Aoki, Player position estimation by monocular camera for soccer video analysis, in: *SICE Annual Conference 2011*, IEEE, 2011, pp. 1985–1990.
- [15] M. Hoernig, M. Herrmann, B. Radig, Real time soccer field analysis from monocular TV video data, in: *11th International Conference on Pattern Recognition and Image Analysis (PRIA-11-2013)*, Vol. 2, The Russian Academy of Sciences, 2013, pp. 567–570.
- [16] H. Sabirin, H. Sankoh, S. Naito, Automatic soccer player tracking in single camera with robust occlusion handling using attribute matching, *IEICE TRANSACTIONS on Information and Systems* 98 (8) (2015) 1580–1588.
- [17] A. Cioppa, A. Deliege, M. Van Droogenbroeck, A bottom-up approach based on semantics for the interpretation of the main camera stream in soccer games, in: *Proceedings of the IEEE Conference on Computer Vision and Pattern Recognition Workshops*, 2018, pp. 1765–1774.
- [18] A. Javed, K. M. Malik, A. Irtaza, H. Malik, A decision tree framework for shot classification of field sports videos, *The Journal of Supercomputing* (2020) 1–26.
- [19] M. M. N. Ali, M. Abdullah-Al-Wadud, S.-L. Lee, An efficient algorithm for detection of soccer ball and players, *Proc. 16th ASTL Control and Networking* 16 (2012) 39–46.

- [20] U. Rao, U. C. Pati, A novel algorithm for detection of soccer ball and player, in: 2015 International Conference on Communications and Signal Processing (ICCSP), IEEE, 2015, pp. 0344–0348.
- [21] S. Sarkar, A. Chakrabarti, D. P. Mukherjee, Generation of ball possession statistics in soccer using minimum-cost flow network, in: 2019 IEEE/CVF Conference on Computer Vision and Pattern Recognition Workshops (CVPRW), 2019, pp. 2515–2523.
- [22] T. Rianthong, S. Thewsuwan, T. Charoenpong, K. Pattanaworapan, A method for detecting lines on soccer field by color of grass variation, in: 2020 12th International Conference on Knowledge and Smart Technology (KST), IEEE, pp. 131–134.
- [23] Y. Qian, D. D. Lee, Adaptive field detection and localization in robot soccer, in: Robot World Cup, Springer, 2016, pp. 218–229.
- [24] D. Quilón, R. Mohedano, C. Cuevas, N. García, Unsupervised high-quality soccer field segmentation, in: International Symposium on Consumer Electronics (ISCE), IEEE, 2015, pp. 1–2.
- [25] J. Bu, S. Lao, L. Bai, Automatic line mark recognition and its application in camera calibration in soccer video, in: 2011 IEEE International Conference on Multimedia and Expo, IEEE, 2011, pp. 1–6.
- [26] Y. Yang, D. Li, Robust player detection and tracking in broadcast soccer video based on enhanced particle filter, *Journal of Visual Communication and Image Representation* 46 (2017) 81–94.
- [27] D. A. Sadlier, N. E. O’Connor, Event detection in field sports video using audio-visual features and a support vector machine, *IEEE Transactions on Circuits and Systems for Video Technology* 15 (10) (2005) 1225–1233.
- [28] I. Jabri, et al., Camera calibration using court models for real-time augmenting soccer scenes, *Multimedia Tools and Applications* 51 (3) (2011) 997–1011.
- [29] J.-B. Hayet, J. H. Piater, J. G. Verly, Fast 2D model-to-image registration using vanishing points for sports video analysis, in: IEEE International Conference on Image Processing 2005, Vol. 3, IEEE, 2005, pp. 417–420.
- [30] N. Homayounfar, S. Fidler, R. Urtasun, Sports field localization via deep structured models, in: Proceedings of the IEEE Conference on Computer Vision and Pattern Recognition, 2017, pp. 5212–5220.
- [31] L. Alvarez, V. Caselles, Homography estimation using one ellipse correspondence and minimal additional information, in: 2014 IEEE International Conference on Image Processing (ICIP), IEEE, 2014, pp. 4842–4846.

- [32] P. Mukhopadhyay, B. B. Chaudhuri, A survey of Hough transform, *Pattern Recognition* 48 (3) (2015) 993–1010.
- [33] L. Xu, E. Oja, P. Kultanen, A new curve detection method: randomized Hough transform (RHT), *Pattern recognition letters* 11 (5) (1990) 331–338.
- [34] J. R. Bergen, H. Shvaytser, A probabilistic algorithm for computing Hough transforms, *Journal of algorithms* 12 (4) (1991) 639–656.
- [35] K. Wan, L. Joo-Hwee, C. Xu, X. Yu, Real-time camera field-view tracking in soccer video, in: 2003 IEEE International Conference on Acoustics, Speech, and Signal Processing, 2003. Proceedings.(ICASSP'03)., Vol. 3, IEEE, 2003, pp. 185–188.
- [36] Y. Wu, H. Wang, F. Tang, Z. Wang, Efficient conic fitting with an analytical Polar-N-Direction geometric distance, *Pattern Recognition* 90 (2019) 415–423.
- [37] H. Akaike, A new look at the statistical model identification, *IEEE Transactions on Automatic Control* 19 (6) (1974) 716–723. doi:10.1109/TAC.1974.1100705.
- [38] G. Gallego, C. Cuevas, R. Mohedano, N. Garcia, On the Mahalanobis distance classification criterion for multidimensional normal distributions, *IEEE Transactions on Signal Processing* 61 (17) (2013) 4387–4396.
- [39] J. C. Maxwell, On hills and dales, *The London, Edinburgh, and Dublin Philosophical Magazine and Journal of Science* 40 (269) (1870) 421–427. doi:10.1080/14786447008640422.
- [40] S. Beucher, C. Lantuéjoul, Use of watersheds in contour detection, in: Proceedings of the International Workshop on Image Processing, CCETT, 1979, pp. 2.1–2.12.
- [41] S. Beucher, F. Meyer, The morphological approach to segmentation: the watershed transformation, *Mathematical morphology in image processing* 34 (1993) 433–481.
- [42] R. Barnes, C. Lehman, D. Mulla, Priority-flood: An optimal depression-filling and watershed-labeling algorithm for digital elevation models, *Computers & Geosciences* 62 (2014) 117–127. doi:<https://doi.org/10.1016/j.cageo.2013.04.024>.
- [43] J. Cousty, G. Bertrand, L. Najman, M. Couprise, Watershed cuts: minimum spanning forests and the drop of water principle, *IEEE Transactions on Pattern Analysis and Machine Intelligence* 31 (8) (2009) 1362–1374.
- [44] F. Malmberg, C. L. Luengo Hendriks, An efficient algorithm for exact evaluation of stochastic watersheds, *Pattern Recognition Letters* 47 (2014) 80–84, advances in Mathematical Morphology. doi:<https://doi.org/10.1016/j.patrec.2014.03.016>.

- [45] S. C. Tolosa, S. Blacher, A. Denis, A. Marajofsky, J.-P. Pirard, C. J. Gommes, Two methods of random seed generation to avoid over-segmentation with stochastic watershed: application to nuclear fuel micrographs, *Journal of Microscopy* 236 (1) (2009) 79–86. doi:10.1111/j.1365-2818.2009.03200.x.
- [46] R. Bridson, Fast Poisson disk sampling in arbitrary dimensions, in: *ACM SIGGRAPH 2007 Sketches*, Association for Computing Machinery, New York, NY, USA, 2007, p. 22. doi:10.1145/1278780.1278807.
- [47] D. Bradley, G. Roth, Adaptive thresholding using the integral image, *Journal of Graphics Tools* 12 (2) (2007) 13–21. doi:10.1080/2151237X.2007.10129236.
- [48] F. Meyer, Iterative image transformations for an automatic screening of cervical smears., *Journal of Histochemistry & Cytochemistry* 27 (1) (1979) 128–135. doi:10.1177/27.1.438499.